Quantum/Classical Studies of Vibrationally Mediated Photodissociation of Ar·H_2O†

Feng Chen and Anne B. McCoy*

Department of Chemistry, The Ohio State University, Columbus, Ohio 43210

Received: March 30, 2008; Revised Manuscript Received: June 15, 2008

Results of multiple configuration quantum/classical simulations of the dynamics of Ar·H_2O photodissociation are reported. In agreement with experimental studies of Nesbitt and co-workers [*J. Chem. Phys.* **2000**, *112*, 7449], we find that the OH products emerge rotationally excited, compared to the dissociation of bare H_2O. The wavelength dependence of the total cross section and the energy transfer to the argon atom are also investigated. The trends are interpreted in terms of features in the Ar·H_2O $\tilde{A}$ state potential surface.

Introduction

Solvation can have a variety of influences on chemical reaction dynamics. Introducing additional chemical species can favor a particular channel, while closing others. The introduction of a single solvating atom or molecule can have a measurable effect on the energy distribution among the products of unimolecular or bimolecular reactions in the gas phase.[1–12] In the present work we focus on one of the simplest types of chemical processes, photodissociation, and on solvation by a single argon atom. This work is motivated by a series of experimental studies on this system by Nesbitt and co-workers[1–4] and the classical studies of Christoffel and Bowman.[5]

In addition to our goal of better understanding the dynamics of UV photodissocation of Ar·H_2O complexes, we are interested in understanding how well quantum/classical approaches will describe such processes. Here, the relatively small size of the system allows for detailed experimental measurements of quantities such as rotation/vibration product state distributions. On the other hand, fully quantum mechanical simulations are challenging for this process. Although quantum approaches have been used to study the dynamics of reacting systems with as many as five atoms or seven internal degrees of freedom, including the H + H_2O,[13] OH + CO,[14,15] O(^{3}P) + CH_4,[16,17] and H + HCN[18] reactions, photodissociation of Ar·H_2O introduces several additional challenges. First, in contrast to the above systems, Ar·H_2O dissociates into three products, H + OH + Ar, along two reactive channels. Further, the energy that is imparted on the dissociating hydrogen atom can exceed 1.7 eV.

In processes, like the photodissociation of H_2O, where there are two equivalent channels (arising from the equivalence of the two OH bonds in water), traditional quantum/classical approaches are destined to fail due to the overcorrelation between the quantum and classical dynamics.[19,20] We developed and tested a multiple configuration extension to the quantum/classical approach in which the quantum wave packet is projected onto two or more channels and the forces felt by the classical particles are based on averages of the gradient of the potential over the probability amplitude in one of these channels.[21–26] This removes many of the problems with overcorrelation in the quantum/classical approach, without significantly increasing the computational expense. We have applied this approach to studies of reactions of O(^{3}P) with HCl and Ar·HCl,[23,24] and the photodissociation of water[25] and Ar·H_2O[26] in its ground vibrational state. In the present study, we focus on the photodissociation dynamics of Ar·H_2O from vibrationally excited states of water. In particular, we investigate the energy transfer dynamics of this process and how it is reflected in the OH rotational energy, as this is a quantity that has been reported by Nesbitt and co-workers in the case when three quanta are put into one of the OH stretches in Ar·H_2O prior to UV photodissocation.[4]

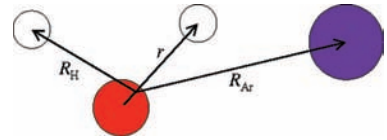

Figure 1. Illustration of the satellite coordinates used in this study. The white circles represent the two hydrogen atoms, the purple circle represents the argon atom, and the red circle represents the oxygen atom.

The remainder of the paper is organized as follows. In the following section, we review the Hamiltonian and the quantum/classical approaches we use in this work. More detailed accounts of these approaches can be found in refs 20, 25 and 26, In section III, we report the results for the photodissociation of H_2O from its second overtone. In section IV, results for vibrationally mediated photodissociation of water from the excited states with three or four quanta in one OH stretch, as well as the combination band with three quanta in one OH stretch and one in the other are reported and contrasted. A summary is given in section V.

Coordinates and Hamiltonian

As in our previous studies of the Ar·H_2O system,[26] we express the dynamics in the planar satellite coordinates.[20,27,28] As is illustrated in Figure 1, the positions of one of the hydrogen atoms and the argon atom are referenced to the center of mass of the OH bond. In these coordinates, the Hamiltonian is given by

$$\hat{H} = \frac{\hat{\mathbf{p}}_r^2}{2\mu_{OH}} + \frac{\mathbf{P}_H^2}{2\mu_{H-OH}} + \frac{\mathbf{P}_{Ar}^2}{2\mu_{Ar-OH}} + \frac{\mathbf{P}_{Ar}\cdot\mathbf{P}_H}{m_H + m_O} + V(\mathbf{r},\mathbf{R}_H,\mathbf{R}_{Ar}) \quad (1)$$

where μ_r is the reduced mass of OH, μ_{X-OH} is the reduced mass associated with the X−OH vector. The intermolecular potential

† Part of the "Stephen R. Leone Festschrift".

* Corresponding author. E-mail: mccoy@chemistry.ohio-state.edu.

10.1021/jp8027287 CCC: $40.75
Published on Web 08/16/2008

is given by $V(\mathbf{r},\mathbf{R}_H,\mathbf{R}_{Ar})$ and $\mathbf{p}_r$, $\mathbf{P}_H$ and $\mathbf{P}_{Ar}$ are the momenta conjugate to the three vectors illustrated in Figure 1. The final term in the Hamiltonian is the potential surface for $Ar\cdot H_2O$. For the $\tilde{X}$ state, we use the ab initio surface of Partridge and Schwenke[29] to describe the intramolecular water potential and the surface of Cohen and Saykally[30] to describe the $Ar-H_2O$ intermolecular interactions. For the $\tilde{A}$ state, we use the additive potential developed by Christoffel and Bowman.[5] This potential is based on the $\tilde{A}$ state H_2O potential of Schinke and coworkers.[31] The intermolecular interactions are described by the Ar−OH $\tilde{X}$ state potential of Lester et al.[32] and the Ar−H potential of Tang and Toennies.[33] To ensure that the potential dissociates properly, the Ar + H + OH′ and Ar + OH + H′ intermolecular potentials are combined using a cubic switching function.[5]

In earlier work, we showed that many of the important features of the dynamics can be obtained by constraining the motion to a plane, without significant loss of accuracy.[26] In this representation,

$$\hat{\mathbf{p}}_r^2 = -\hbar^2\left(\frac{\partial^2}{\partial r^2} + \frac{1}{4r^2} + \frac{1}{r^2}\frac{\partial^2}{\partial\theta^2}\right) \tag{2}$$

where r is the magnitude of $\mathbf{r}$ and θ gives the angle between r and the space-fixed X axis.

We will compare the results to those obtained for the dissociation of an isolated water molecule. Because the quantum-classical and planar treatments introduce some approximations to the dynamics, we treat the H_2O dynamics in a parallel manner. This is achieved by taking the $\mathbf{R}_{Ar}\rightarrow\infty$ limit of the Hamiltonian in eq 1. This results in a separable Hamiltonian and only the dynamics in r and $\mathbf{R}_H$ need be propagated in this case.

As in our previous studies of H_2O and $Ar\cdot H_2O$, we treat the dynamics in r quantum mechanically, whereas the dynamics in $\mathbf{R}_H$ and $\mathbf{R}_{Ar}$ are treated classically. In the simplest quantum/classical treatment, the quantum wave packet is propagated using a time-dependent Hamiltonian, evaluated at the positions and momenta of the classical particles. The dynamics of the classical particles are then evaluated using the average of $-\partial V/\partial x_\alpha$, where the average is over the probability distribution derived from the quantum wave packet at time t. This can be very accurate as long as the wave packet remains localized. If the wave packet spreads or bifurcates, so as to sample regions of the potential that exert different forces on the classical particles, serious errors can result.

To reduce this problem, we developed a multiple-configuration quantum/classical approach, based on the work of Wang and Clary.[21] A derivation of our approach has been reported previously.[20] The basic idea is to project the quantum wave packet onto distinct configurations and propagate separate classical trajectories for each of the configurations. In the present work, we employ a two configuration treatment. One configuration corresponds to breaking the OH bond that is described by $\mathbf{R}_H$ and another in which the OH bond that is described by $\mathbf{r}$ is broken. Because the OH bond that is not broken is expected to exhibit the largest quantum mechanical effects, we focus our analysis on the first of the two configurations. This leads to the set of coupled equations:

$$i\hbar\frac{\partial\chi(\mathbf{r},t)}{\partial t} = \left\{\frac{\mathbf{p}_r}{2\mu_{OH}} + V(\mathbf{r},\mathbf{R}_H(t),\mathbf{R}_{Ar}(t))\right\}\chi(\mathbf{r},t)$$

$$\frac{d\mathbf{R}_H}{dt} = \frac{\mathbf{P}_H(t)}{\mu_{H-OH}} + \frac{\mathbf{P}_{Ar}(t)}{m_H + m_O}$$

$$\frac{d\mathbf{R}_{Ar}}{dt} = \frac{\mathbf{P}_{Ar}(t)}{\mu_{Ar-OH}} + \frac{\mathbf{P}_H(t)}{m_H + m_O}$$

$$\frac{dP_\alpha^{(n)}}{dt} = -\frac{\langle\chi_n(\mathbf{r},t)|\frac{\partial V}{\partial X_\alpha}|\chi_n(\mathbf{r},t)\rangle}{\langle\chi_n(\mathbf{r},t)|\chi_n(\mathbf{r},t)\rangle} \tag{3}$$

where α represents one of the components of $\mathbf{R}_H$ or $\mathbf{R}_{Ar}$ and n describes the channel for which the classical dynamics is propagated. Operationally,

$$|\chi_1\rangle = \sum_{j=0}^{4}|\phi_j\rangle\langle\phi_j|$$

$$|\chi_2\rangle = \sum_{j=5}^{\infty}|\phi_j\rangle\langle\phi_j| \tag{4}$$

where $\phi_j(\mathbf{r})$ provides the asymptotic, j_{OH}, OH wave functions.

The initial conditions are obtained in two steps. In the absence of the argon atom, the two OH bonds in water are equivalent, by symmetry, and the eigenstates are well-described by sums and differences of pairs of local mode states. For the three states that are the focus of present study, the energy splittings for the pairs of eigenstates are 14 and 2 for the overtones with three and four quanta in one of the OH stretches and 98 for the combination band in which one OH stretch has three quanta of excitation and the other has one quantum.[29] This leads us to expect that the coupling between the corresponding local mode states should be small, particularly for the two overtones. When an argon atom is introduced, it will break the symmetry of the water OH stretch vibrations and the eigenstates will no longer be equal admixtures of the localized states.

As such, for our initial conditions for H_2O, we use the sums and differences of the eigenstates of water, calculated from the Partridge and Schwenke potential.[29] These are denoted by

$$|n\rangle_r|m\rangle_R|l\rangle_\theta = \frac{1}{\sqrt{2}}[|mn\rangle^+ \pm |mn\rangle^-]|l\rangle \tag{5}$$

where n provides the number of quanta in the OH bond that is described by $\mathbf{r}$, m provides the number of quanta in the OH bond described by $\mathbf{R}_H$ and l gives the number of quanta in the bend. The wave function, though roughly separable, is still coupled and the $|mn\rangle^\pm|l\rangle$ notation is used to describe the eigenstates. To obtain initial conditions for the quantum/classical simulations, we will need to separate the $\mathbf{R}_H$ dependence of the wave function from its dependence on r and θ. This is achieved through a natural modal analysis,[34] as described in refs 25 and 35.

The natural modal analysis yields a separable wave function of the form

$$\psi(r,R_H,\theta) = \phi(r,\theta)\,\chi(R_H) \tag{6}$$

for which the overlap with the full coupled wave function is maximized. In the quantum/classical treatment of the dynamics in r and θ is propagated quantum mechanically, while the dynamics in $\mathbf{R}_H$ and $\mathbf{P}_H$ is propagated classically. The initial conditions in r and θ are given by $\phi(r,\theta)$, whereas the initial values of the X component of $\mathbf{R}_H$ and $\mathbf{P}_H$ are selected at random from each square on a 80×80 grid that encompasses the region of phase space over which the Wigner function

$$W(R,P) = \frac{1}{2\pi\hbar}\int_{-\infty}^{\infty}ds\,\chi^*\left(R+\frac{s}{2}\right)\chi\left(R-\frac{s}{2}\right)e^{isP/\hbar} \tag{7}$$

has amplitude. As in our previous work, the Y components of these vectors are initially set equal to 0. The value of the Wigner

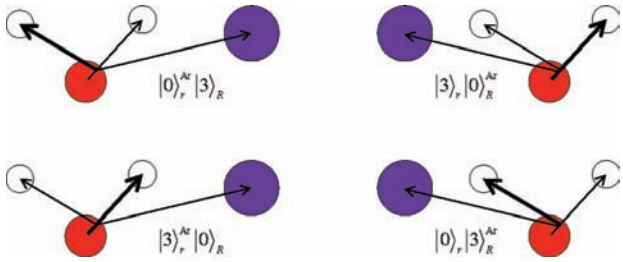

Figure 2. Four possible configurations of the state of Ar·H2O with three quanta in one OH bond and zero in the other. The thick vector indicates which OH bond contains the greater vibrational excitation, and the notation used in the text is indicated on each of the four panels. As in Figure 1, the hydrogen atoms are represented with white circles, the oxygen atom by a red circle and the argon atom by a larger purple circle.

distribution function at the initial classical coordinates and momentum is used to weight the trajectory. The initial position of the argon atom is taken to be its minimum energy configuration. Note that although the argon position is fixed relative to the center of mass of OH, the quantum nature of the treatment of **r** means that a range of geometries are, in fact, sampled.

For the $|n\rangle_r|m\rangle_R|l\rangle_\theta$ initial state, there are two possible positions for the argon atom. It can be closer to either the OH bond that is treated classically or the OH bond that is treated quantum mechanically. As such, for a state of Ar·H2O with i quanta in one OH stretch and j quanta in the other, there are four possible situations. These are denoted by $|i\rangle_r|j\rangle_R^{Ar}$,$|i\rangle_r^{Ar}|j\rangle_R$,$|j\rangle_r^{Ar}|i\rangle_R$ and $|j\rangle_r|i\rangle_R^{Ar}$. Taken together, they will be referred to as the $|i, j\rangle$ family of states. The $|3, 0\rangle$ family is illustrated in Figure 2. We have not included the number of quanta in the bend in the above and subsequent notation because in all cases there will be zero quanta initially in this mode.

The quantities that we focus on below will be the total cross section and the rotational energy of the OH products. The equations used to derive these quantities have been presented previously and will not be repeated here.[26] We also investigate the energy transfer to the argon atom.

Photodissociation Dynamics of Water

Before discussing the Ar·H2O photodissociation dynamics, we consider the water system where we can make comparisons between the quantum/classical and three-dimensional quantum simulations. The symmetrized and unsymmetrized representations of the state with three quanta in one of the OH bonds are illustrated in Figure 3. As seen in these plots, the localized states are separable into one OH stretch with three quanta and the other has zero quanta. Although the total cross sections for each of these states is quantitatively different, if we average the cross sections, obtained when we start in the two normal mode states plotted in Figure 3a,b, we find that the result is nearly identical to the total cross section for either of the local modes states.[35] Similar agreement is found when the total cross sections are broken down into partial cross sections to specific rotation−vibration states. This may be surprising, as one would expect that quantum interference effects could play a role in the dynamics. The fact that the dissociation dynamics is direct and prompt is responsible for this relatively simple additive behavior. In addition, we find that the local mode cross section is much larger when the OH bond with three quanta is broken than when the bond with no quanta is broken. This is exactly what was reported by Crim and co-workers in their studies of vibrationally mediated photodissociation of this system.[36] This is also consistent with physical intuition which says that putting energy

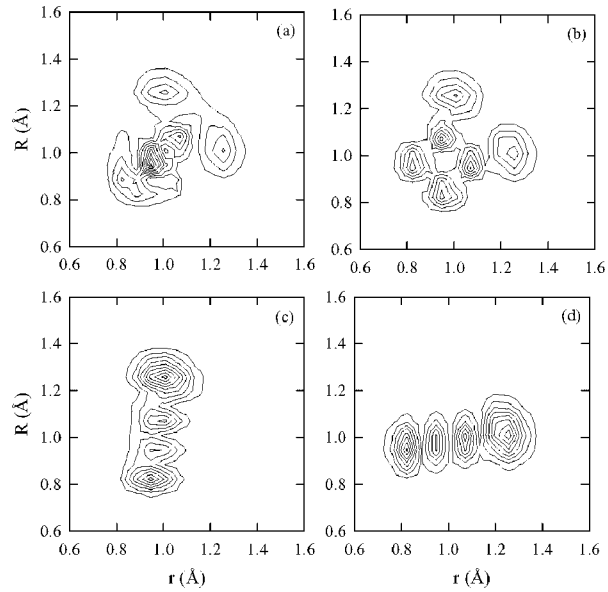

Figure 3. Stretch wave functions for the (a) $|30\rangle^+|0\rangle$, (b) $|30\rangle^-|0\rangle$, (c) $|0\rangle_r|3\rangle_R|0\rangle_\theta$ and (d) $|3\rangle_r|0\rangle_R|0\rangle_\theta$ states of H2O.

into one of the bonds, through vibrational excitation, will make it easier to break that bond.

Previous comparisons of the quantum and quantum/classical cross sections for the photodissociation of water indicate good agreement.[25,26] Similar agreement was found when we performed these comparisons for the present simulations.

Photodissociation Dynamics of Argon−Water Complexes

In considering the photodissociation of Ar·H2O, we focus on three sets of states: the $|3, 0\rangle$ family of states, which have been studied by Nesbitt and co-workers, as well as the $|4, 0\rangle$ and $|3, 1\rangle$ families. Each of these families is composed of two possible configurations at $t = 0$. One has the argon atom closer to the more highly excited OH bond. For the geometries shown in Figure 2 these correspond to the $|3\rangle_r^{Ar}|0\rangle_R$ and $|0\rangle_r|3\rangle_R^{Ar}$ cases. The second possibility puts the argon atom nearer the OH bond with less vibrational excitation, the $|0\rangle_r^{Ar}|3\rangle_R$ and $|3\rangle_r|0\rangle_R^{Ar}$ cases in Figure 2.

In studies of the $|3, 0\rangle|0\rangle$ band of Ar·H2O by Nesbitt and co-workers,[1] it was found that the frequency of this transition is shifted by 3.12 cm^{-1}, compared to the corresponding transition in water. This indication that the OH stretch that is excited is only weakly perturbed by the interaction with the argon atom motivates the model we have adopted in which the initial conditions for the water molecule and the argon atom are obtained independently.

In Figure 4a, we plot the total cross sections for the four cases illustrated in Figure 2. The two plots shown with solid lines reflect the two cases in which the argon atom is closer to the OH bond that has three quanta of vibrational excitation, with the red line corresponding to the case when this bond is broken. Likewise, the dashed lines give the results when the argon atom is closer to the OH bond with less vibrational excitation. As can be seen, when the OH stretch with vibrational excitation is broken (shown with red lines), the resulting cross section is larger and more structured. The overall contour is similar for the two argon atom positions, although a slight blue shift is seen when the argon-bound OH bond is broken. Although we treat the four cases separately in the calculations, experimentally, for a given Ar−HOH conformer, one cannot select which bond will break.

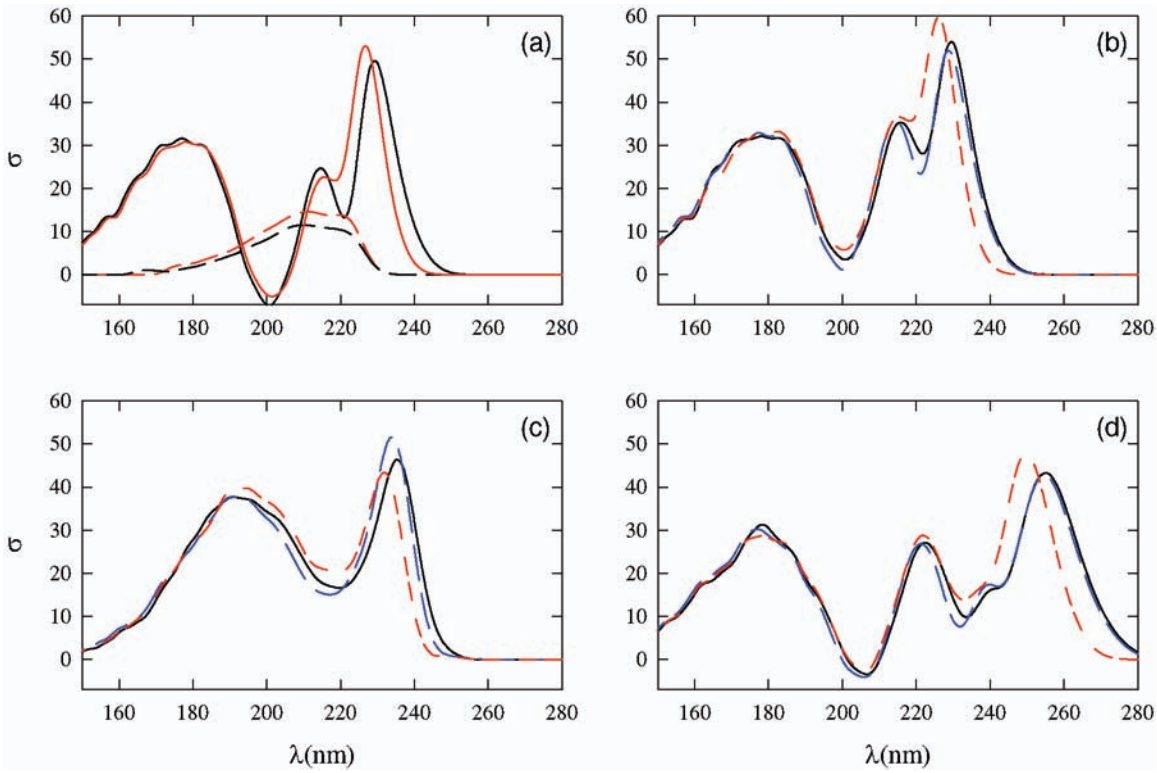

Figure 4. Quantum/classical cross sections for (a) the four cases that make up the $|3, 0\rangle$ set of states, and comparisons of the Ar·H_2O and H_2O cross sections for the (b) $|3, 0\rangle$, (c) $|3, 1\rangle$ and (d) $|4, 0\rangle$ states. In (a) red and black indicate if the vibrationally excited OH bond is argon-bound or free. The solid and dashed lines differentiate the cases when the bond with three quanta of excitation is broken (solid) or the one with no quanta of excitation is broken (dashed). In the remaining three panels, the black curve gives the cross section for bare water, the blue curve is for the case where the free OH stretch is vibrationally excited, and the red curve provides the cross section when the argon-bound OH stretch is vibrationally excited.

In panels b−d of Figure 4, we plot the total cross sections for the two distinct cases for the $|3, 0\rangle$, $|3, 1\rangle$ and the $|4, 0\rangle$ initial states of water. The results for bare water are plotted with black lines, for comparison. In all cases, we note a small red shift in the cross section when the argon atom is closer to the OH bond that has less excitation. When the argon atom is nearer to the OH bond that is excited, the cross section displays a blue shift. This blue shift is largest at the long wavelengths and is negligible for wavelengths below ≈190 nm. The blue shifts of the peak near 230 nm are quantified in Table 1.

The source of this blue shift can be understood by realizing that the primary contribution to the cross section in this spectral region comes from breaking the more vibrationally excited OH bond. The blue shift is observed when the argon atom is closer to this bond and reflects the repulsive interaction between the argon and hydrogen atom. The fact that the shift is larger when there are initially four quanta in the OH bond than when there are three, indicates that the blue shift also increases with increasing OH bond extension. To quantify this, we consider the average value of the intermolecular Ar·H_2O $\tilde{A}$ state potential,

$$\bar{R}_{\tilde{A}} = \langle \chi | V^{\tilde{A}}_{Ar\cdot H_2O} | \chi \rangle_{R_H > R_t} = \frac{\int_{R_t}^{\infty} dR_H \, |\chi(R_H)|^2 V^{\tilde{A}}_{Ar\cdot H_2O}}{\int_{R_t}^{\infty} dR_H \, |\chi(R_H)|^2} \quad (8)$$

where R_t is chosen so that the integral is over the right-most peak in the probability distribution in R. Specifically, $R_t = 2.24$ a_0 for the $|3, 0\rangle$ and the $|3, 1\rangle$ states and 2.35 a_0 for the $|4, 0\rangle$ state. The potential is obtained by setting the position of the argon atom and the OH bond that is not broken to their equilibrium values, and changing the value of only R_H. As can be seen in the results reported in Table 1, this simple picture reproduces the calculated blue shifts.

TABLE 1: Blue Shifts in the Photodissociation Cross Sections for Ar·H_2O Compared to Bare H_2O

state	blue shift (cm^{-1})	$\bar{V}_{\tilde{A}}$ (cm^{-1})[a]
$\|3, 0\rangle\|0\rangle$	658	630.3
$\|3, 1\rangle\|0\rangle$	654	662.8
$\|4, 0\rangle\|0\rangle$	831	900.4

[a] Defined in eq 8.

Although the blue shifts are interesting, another experimental observable for these systems is the rotational energy in the OH product. In Figure 5, we plot the average OH rotational energy as a function of wavelength the (a) $|3, 0\rangle$ and (b) $|4, 0\rangle$ states and compare them to the corresponding values for the photodissociation of H_2O at the same wavelength. In these plots we have distinguished between the cases in which the argon-bound OH stretch is vibrationally excited and that in which the free OH bond has the vibrational excitation. At wavelengths below 240 nm, the results of Figure 5 show that if we start from either of these states, the OH products will end up hotter than if the argon had not been present.

For longer wavelengths, the situation changes. At these wavelengths, there is not sufficient energy to break the bond that initially had zero-quanta. We find that the OH products that are obtained when the free OH bond is broken are hotter than those obtained from photodissociation of bare water whereas, in the case in which the argon-bound OH bond in water is broken, the rotational distribution is somewhat colder than in bare water.

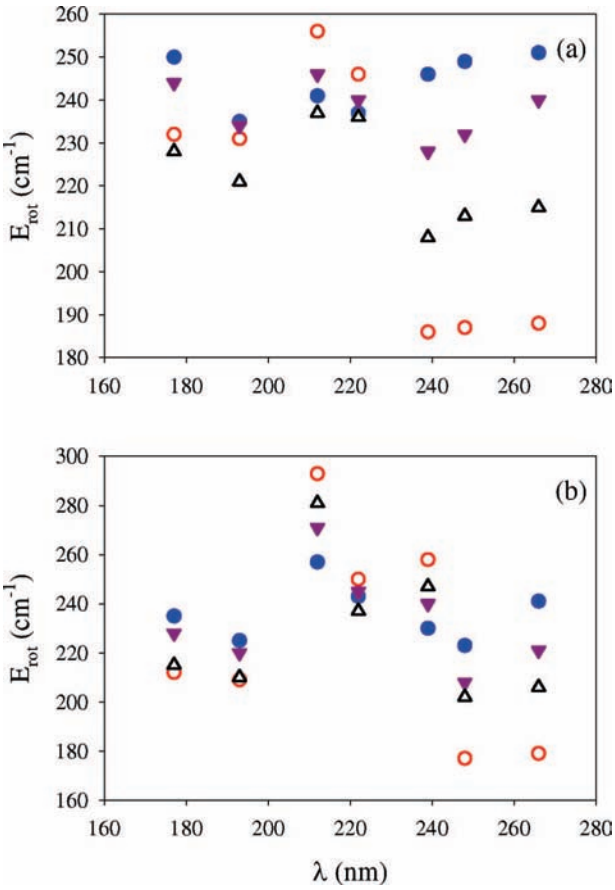

Figure 5. Average rotational energies following photodissociation from the (a) $|3, 0\rangle$ and (b) $|4, 0\rangle$ states. Filled blue and opened red circles denote cases where the free and argon-bound OH stretches are vibrationally excited. Filled purple triangles represent the average of these quantities, and open black triangles provide the corresponding averages for photodissociation of bare water.

The only experimental measurement to which we can compare these results comes from the work of Nesbitt and coworkers.[4] They found that photodissocation of Ar·H_2O at 248 nm resulted in an average OH rotational energy of 134 cm^{-1}, compared to an average of 96 cm^{-1} for the uncomplexed water molecule. Comparison to our results for this wavelength requires knowledge of which OH bond is broken. Based on the cross sections, plotted in Figure 4, it appears that at this wavelength the cross section for breaking the free OH bond is much larger than that for breaking the argon-bound one. This being the case, we predict a larger rotational energy of the OH products, which is consistent with the experiment. Clearly the order of magnitude of the effect is not in as good agreement as we would like. Given the additive nature our model for the Ã state potential, we would have been surprised if we had obtained quantitative agreement.

As we analyze the trends, the differences in the rotational energy at the longer wavelengths is surprising but can be understood by considering the Ar·OH Ã state potential, plotted in Figure 6. Superimposed on this plot is the initial position of the OH bond and the direction of its momentum vector. From the arrows, we see that when the argon atom is nearer the OH bond that is broken, the remaining OH molecule is pushed away from the argon atom and rapidly reaches parts of the potential for which the interaction is nearly isotropic. As a result, the argon atom is expected to have little effect on the rotational distribution of the OH product. At longer wavelengths, the remaining OH comes off with a smaller amount of kinetic

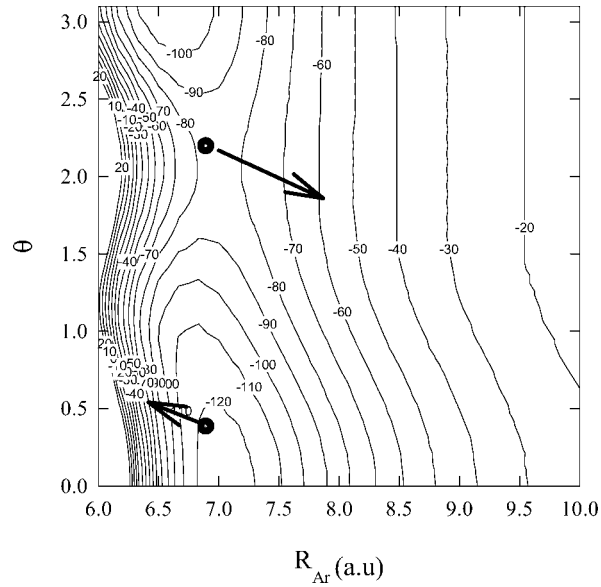

Figure 6. Contour plot of the potential for Ar·OH.[32] The contours are plotted for energies from −120 to +20 cm^{-1} in increments of 10 cm^{-1}. The two dots represent initial position of the argon atom when it is bound to the OH bond that is broken and when it is bound to the OH bond that remains intact. The arrows provide the direction of the OH momentum vector at $t = 0$.

energy, leading to a longer-lived Ar−OH complex and lower final rotational energy for the OH product.

In the other case, the remaining OH molecule is pushed toward the argon by the H−OH repulsive force and it samples the highly anisotropic repulsive wall on the potential. A torque is imposed on the OH bond, leading to an increase in the average angular momentum of the OH product. The anisotropy of the potential that is sampled will be sensitive to the available energy.

As is seen in Figure 4, breaking the OH bond with more quanta has a much larger contribution to the total cross section at longer wavelengths. Consequently, one would expect that the rotational distributions of the OH product would provide a way to probe of which OH bond has been broken.

Finally, we consider energy transfer to the argon atom, averaged over all excitation wavelengths. The results are plotted in Figure 7. To help in the interpretation of the results, we have separated the contributions into two curves. The blue curves represent the distriutions when the free OH stretch is vibrationally excited (depicted in the lower panels of Figure 2), and the red curves provide the distributions that are obtained when the argon-bound OH stretch is vibrationally excited (depicted in the lower panels of Figure 2). In all cases, there are two peaks in these distributions. One is centered at the origin, and the other is broader and is centered near 800 cm^{-1}. On the basis of the conservation of linear momentum and energy, when one of the OH bonds in H_2O is broken, most of the kinetic energy is imparted on the dissociating hydrogen atom. Classically, either OH bond can break. Quantum mechanically, both will occur, although the relative cross sections will depend on the total available energy and, at most wavelengths, the more vibrationally excited OH bond will be more easily broken. When the OH bond that is further from the argon atom is broken, little kinetic energy will be transferred to the argon atom. This case corresponds to the peak near 0 cm^{-1} in Figure 7. When the other OH bond is broken, the hydrogen atom will pass close to the argon atom and there is significant energy transferred between these two atoms. This leads to the broad peaks in the distributions at 400−1200 cm^{-1}. Further analysis of these plots

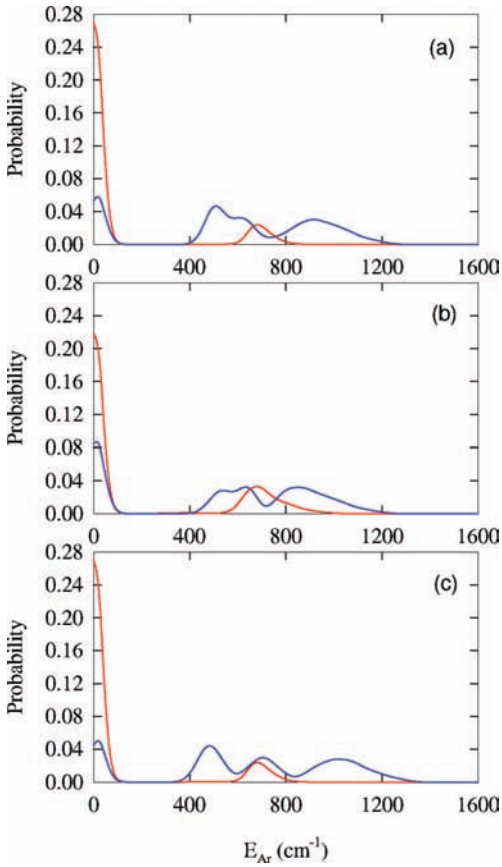

Figure 7. Average kinetic energy of the Ar atom plotted for the (a) $|3, 0\rangle$, (b) $|3, 1\rangle$ and (c) $|4, 0\rangle$ states. In all cases the blue curve results from the case where the free OH stretch is vibrationally excited and the red curve provides the probability when the argon-bound OH stretch is vibrationally excited.

shows that the structure reflects the oscillations in the vibrational wave function.

Conclusions

In this paper, we presented the results of a multiple-configuration quantum/classical study of vibrationally mediated photodissociation of $Ar \cdot H_2O$, focusing on three sets of initial states. We find that the presence of the argon atom causes a blue shift in the total cross section near 240 nm. The introduction of the Ar atom also affects the average rotational energy of the remaining OH product and the calculated trends are consistent with the experimental measurements of this system. The above trends were rationalized in terms of features of the potential energy surfaces. Finally, though the energies of the argon atoms may be challenging to measure experimentally, studies of the kinetic energy distributions of the hydrogen atom by Rydberg tagging techniques could shed light onto the dynamics of this photodissociation process. On the basis of our results, we believe that the photodissciation of $Ar \cdot H_2O$ remains an interesting system and one for which it would be interesting to see future experimental studies.

Acknowledgment. This work was supported by the National Science Foundation through Grant numbers CHE-0200968 and CHE-0515627.

References and Notes

(1) Plusquellic, D. F.; Votava, O.; Nesbitt, D. J. *J. Chem. Phys.* **1994**, *101*, 6356.
(2) Plusquellic, D. F.; Votava, O.; Nesbitt, D. J. *J. Chem. Phys.* **1997**, *107*, 6123.
(3) Fair, J. R.; Nesbitt, D. J. *J. Chem. Phys.* **2000**, *113*, 10962.
(4) Votava, O.; Plusquellic, D. F.; Myers, T. L.; Nesbitt, D. J. *J. Chem. Phys.* **2000**, *112*, 7449.
(5) Christoffel, K. M.; Bowman, J. M. *J. Chem. Phys.* **1996**, *104*, 8348.
(6) Picconatto, C. A.; Ni, H.; Srivastava, A.; Valentini, J. J. *J. Chem. Phys.* **2001**, *114*, 7073.
(7) Wittig, C.; Sharpe, S.; Beaudet, R. A. *Acc. Chem. Res.* **1988**, *21*, 341.
(8) Zhang, J.; Dulligah, M.; Segall, J.; Wen, Y.; Wittig, C. *J. Phys. Chem.* **1995**, *99*, 13680.
(9) Liu, K.; Kolessov, A.; Partin, J. W.; Bezel, I.; Wittig, C. *Chem. Phys. Lett.* **1999**, *299*, 374.
(10) Hurwitz, Y.; Stern, P.; Naaman, R.; McCoy, A. B. *J. Chem. Phys.* **1997**, *106*, 2627.
(11) McCoy, A. B.; Lufaso, M. W.; Veneziani, M.; Atrill, S.; Naaman, R. *J. Chem. Phys.* **1998**, *108*, 9651.
(12) McCoy, A. B.; Naaman, R. *Int. Rev. Phys. Chem.* **1999**, *18*, 459.
(13) Zhang, D. H. *J. Chem. Phys.* **2006**, *125*, 133102.
(14) Balakrishnan, N.; Billing, G. D. *J. Chem. Phys.* **1996**, *104*, 4005.
(15) Valero, R.; Kroes, G.-J. *J. Phys. Chem. A* **2004**, *108*, 8672.
(16) Yang, M.; Lee, S.-Y.; Zhang, D. H. *J. Chem. Phys.* **2007**, *126*, 064303.
(17) Cui, Q.; Wang, M.-L.; Zhang, J. Z. H. *Chem. Phys. Lett.* **2005**, *401*, 115.
(18) Ma, W.-Y.; K.-L. Han, K.-L.; Zhang, J. Z. H. *J. Chem. Phys.* **2002**, *117*, 5642.
(19) Wang, L.; McCoy, A. B. *Phys. Chem. Chem. Phys.* **1999**, *1*, 1227.
(20) McCoy, A. B.; Wang, L.; Chen, F. *Faraday Discuss. Chem. Soc.* **2001**, *118*, 281.
(21) Wang, L.; Clary, D. C. *Chem. Phys. Lett.* **1996**, *262*, 284.
(22) Wang, L. *J. Chem. Phys.* **1998**, *108*, 7538.
(23) Wang, L.; Meurer, W. J.; McCoy, A. B. *J. Chem. Phys.* **2000**, *113*, 10605.
(24) Wang, L.; McCoy, A. B. *J. Chem. Phys.* **2003**, *119*, 1996.
(25) Chen, F.; McCoy, A. B. *J. Phys. Chem. A* **2003**, *107*, 7220.
(26) Chen, F.; McCoy, A. B. *J. Phys. Chem. A* **2004**, *108*, 8819.
(27) McCoy, A. B.; Sibert, E. L. *J. Chem. Phys.* **1996**, *105*, 459.
(28) Mladenovic, M. *J. Chem. Phys.* **2000**, *112*, 1070.
(29) Partridge, H.; Schwenke, D. W. *J. Chem. Phys.* **1997**, *106*, 4618.
(30) Cohen, R. C.; Saykally, R. J. *J. Chem. Phys.* **1993**, *98*, 6007.
(31) Engel, V.; Schinke, R.; Staemmler, V. *J. Chem. Phys.* **1988**, *88*, 129.
(32) Lester, M. I.; Green, W. H.; Chakravarty, C.; Clary, D. C. In *Molecular Dynamics and Spectroscopy by SEP*; Field, R., Dai, H., Eds.; World Scientific Monograph: Singapore, 1995.
(33) Tang, K. T.; Toennies, J. P. *J. Chem. Phys.* **1991**, *156*, 413.
(34) Colbert, D. T.; Sibert, E. L. *J. Chem. Phys.* **1989**, *91*, 350.
(35) Chen, F. Mixed quantum/classical dynamics of photodissociation of H_2O and Ar − H_2O. *PhD thesis*, The Ohio State University, 2004.
(36) Schinke, R.; der Wal, R. L. V.; Scott, J. L.; Crim, F. F. *J. Chem. Phys.* **1991**, *94*, 283.

JP8027287